BUILDING A HETEROGENEOUS Q MODEL: AN APPROACH USING SURFACE REFLECTION DATA

JIN WANG[1,2], WEI LIU[1,2], JIANFENG ZHANG[1] and ZHONGHUA ZHAO[3]

[1] *Institute of Geology and Geophysics, Key Laboratory of Petroleum Resources Research, Chinese Academy of Sciences, Beijing 100029, P.R. China. wangjin112@mails.ucas.ac.cn*
[2] *University of Chinese Academy of Sciences, Beijing 100029, P.R China.*
[3] *Exploration and Development Research Institute, Daqing Oilfield Company Ltd., Daqing 163712, P.R. China.*

(Received August 15, 2016; revised version accepted November 27, 2016)

ABSTRACT

Wang, J., Liu, W., Zhang, J. and Zhao, Z., 2017. Building a heterogeneous Q model: an approach using surface reflection data. *Journal of Seismic Exploration*, 26: 293-310.

The anelasticity of a subsurface medium will cause dissipation of seismic energy. It is challenging to derive an interval Q model in the absence of VSP data and cross-well data. In this paper, we propose a method to derive the Q model using surface reflection data by introducing an effective Q model. Considering the existence of various types of noise, we estimate and evaluate the Q value in terms of compensation effects along with imaging resolution and noise level. Finally, we obtain an optimal compensation result with better resolution and wider bandwidth. Specifically, the effective Q model can be estimated using scanning technology at selected CDP locations to avoid the difficulties of determining a reference event and the thin-bed tuning effect in the conventional spectrum ratio method. The whole Q model can be obtained by a type of interpolation algorithm constrained by geological interfaces, which can be used in the de-absorption prestack time migration directly or in the de-absorption prestack depth migration with the proper time-to-depth conversion. Finally we demonstrate the effectiveness of the proposed approach using a field data example from eastern China. A high-resolution image is obtained.

KEY WORDS: Q model, Q scanning, compensation effects, interpolation algorithm.

INTRODUCTION

Attenuation of seismic waves due to the anelasticity of the subsurface medium can be parameterized by the Q factor in the frequency range of seismic exploration data. It will cause dissipation of seismic energy and loss of high frequencies, thus broadening the propagating wavelet and degrading the resolution of imaging. Some Q-compensating methods, including inverse-Q

0963-0651/17/$5.00

filtering (Bickel and Natargjan, 1985; Hargreaves and Calvert, 1991; Wang, 2002) and viscoelastic migration (Mittet et al., 1995; Zhang and Wapenaar, 2002), can compensate for the amplitudes and correct the phase distortion with an appropriate Q model. Several methods have been developed to estimate the Q value, and most of them count on transmitted waves from the vertical seismic profile (VSP) or cross-well data with less noise. They pick two seismic wavelets from different depths or times and then compare them in the frequency domain and estimate Q based on the changes in the spectra, such as the centroid (Quan and Harris,1997), the peak frequency shift, or the logarithmic spectral area difference (Wang et al., 2015). Although these methods can obtain a Q value with higher accuracy and have some successful applications, they are still limited. The transmitted wave is required to be dominant in the received wavefield and can be separated from the received wavefield. Considering that the real reflection data have a low signal-to-noise ratio (SN), it is still hard to apply this Q model to Q compensation, which will cause high-frequency noise. Furthermore, VSP and cross-well data are not always available or sufficient to build a heterogeneous Q model; thus, we prefer to estimate Q based on surface seismic reflection data.

Some papers have been published concerning the estimation of the Q-factor from the surface reflection data. Dasgupta and Clark (1998) proposed the QVO method using the spectrum-ratio; Zhang and Ulrych (2002) supposed the amplitude spectrum of the seismic wavelet to be Ricker's spectrum and estimated Q according to the peak frequency shift. Two main factors make their methods elusive. One is that it is hard to pick a "clean" wavelet as a reference wavelet spectrum, which is required to come from the shallow layer with less attenuation. The difficulty is that the shallow wavelet attenuates less but is contaminated by environmental noise, surface waves and refracted waves, and it has a low signal-to-noise ratio. The entire estimated Q factor is relative to the reference layer, whose Q value is also not known. The other difficulty is the effects of interference of different seismic arrivals from the thin-bed, which will cause spectral notching, change the locations of peaks or centroid frequency and introduce bias into the results.

We propose a method to build a heterogeneous Q model using surface reflection data. Instead of estimating the interval Q directly, we scan the effective Q (Q_{eff}), which is different from the interval Q, using inverse Q filtering plus prestack migration and choose the suitable Q_{eff} on the performance of the stacked sections. By analyzing the compensated effect in the time-space window, we can avoid the trouble of choosing the reference event in the spectrum ratio method and reduce the side effect of the thin bed interference by changing the location or size of the window. A suitable Qeff compensating section keeps the original structure, blanks the side-lobe of the wavelet, has a higher resolution and can be converted to the interval Q. It is not practical to scan point by point on a 3D survey area, so we focus on the target areas. For

these areas, which are not scanned, Q is obtained by a type of algorithm of interpolation constrained by the geologic model, represented by the velocity model.

The heterogeneous Q-field built by this method has multiple applications. It can be used in the de-absorption prestack time migration directly or in the de-absorption prestack depth migration with proper time-to-depth conversion in order to obtain a high-resolution image.

EFFECTIVE Q AND WAVE COMPENSATION

In an elastic medium, the total energy of a particle is held constant as waves spread away from a localized source region. However, as a wave is propagated through real materials, wave amplitudes attenuate, which can be summarized macroscopically as "internal friction". The attenuation is quantified by the quality factor Q, denoting the ratio of the total energy to energy lost per cycle. Q is taken to be constant or only weakly dependent on the frequency range of observation (Aki and Richards, 1980). To estimate the frequency-dependent Q, we follow Futterman (1962) and Kjartansson (1979) and have the frequency-dependent complex and real phase velocities as

$$\begin{aligned} 1/c(\omega) &= [1/v_r(\omega)][1 - (j/2Q)] \\ v_r(\omega) &= v_r(\omega_c)[1 + (1/\pi Q)\ln(\omega/\omega_c)] \end{aligned} \quad , \tag{1}$$

where ω is the angular frequency, ω_c is the upper cutoff frequency beyond which the real phase velocity approaches a constant, j is the imaginary unit, Q is the quality factor, and $c(\omega)$ and $v(\omega)$ are the complex and real velocity for frequency ω. Introducing the dominant frequency ω_0 and neglecting the high-order terms of 1/Q, the complex velocity is given by

$$1/c(\omega) = (1/v)[1 - (j/2Q)][1 - (1/\pi Q)\ln(\omega/\omega_0)] \quad , \tag{2}$$

where v is the real phase velocity of at the dominant frequency ω_0.

If we were faced with a layered, isotropic and heterogeneous medium, one in which the real velocity and Q were both constants in each layer, we could incorporate the complex velocity into the viscoacoustic phase-shift method to propagate the recorded data downward one layer at a time. The wave field at time depth T in the frequency-wavenumber domain could be written:

$$\begin{aligned} &\tilde{P}(k_x,k_y,\omega,T) \\ &= F(\omega)e^{-jk_x x_g}\, e^{-jk_y y_g}\, e^{j\omega \sum_{i=1}^{n} \Delta T_i[1-2\ln(\omega/\omega_0)/(\pi Q_i)-v_i^2(k_x^2+k_y^2)/\omega^2 \,-\, j/Q_i]^{1/2}} \end{aligned} \quad , \tag{3}$$

where $F(\omega)$ is the Fourier transform of a seismic trace, $T = \Sigma_{i=1}^{n}\Delta T_i$, x_g and y_g are the lateral coordinates of the received trace, ΔT_i is the one-way vertical travel time through each layer that reads $\Delta T_i = \Delta z_i/v_i$, and Δz_i, v_i, and Q_i denote the thickness, velocity and Q of the layer, respectively.

Introducing two effective parameters, Q_{eff} and V_{rms}, that read

$$1/Q_{eff} = (1/T)\sum_{i=1}^{n}\Delta T_i/Q_i \quad \text{and} \quad V_{rms}^2 = (1/T)\sum_{i=1}^{n}\Delta v_i^2 \ , \tag{4}$$

to eq. (3) and then performing a spatial inverse Fourier transform, we have:

$$P(x,y,\omega,T) = (\omega^2/4\pi^2)\iint F(\omega)$$

$$\times\ e^{j\omega T\{\sum [1-2\ln(\omega/\omega_0)/(\pi Q_i)-V_{rms}^2(p_x^2+p_y^2)-j/Q]^{1/2}+p_x(x-x_g)+p_y(y-y_g)\}}$$

$$\times\ e^{(\omega T/2Q_{eff})[1-2\ln(\omega/\omega_0)/(\pi Q_i)-V_{rms}^2(p_x^2+p_y^2)]^{1/2}}\,dp_x dp_y \ , \tag{5}$$

where $p_x = k_x/\omega$ and $p_y = k_y/\omega$ are the ray parameters in the x- and y-directions, respectively.

The integral on the right of eq. (5) can be approximated by a stationary-phase method (Bleistein, 1984), and the downward-continued wavefield is:

$$P(x,y,\omega,T) \approx F(\omega)[\omega/2\pi]e^{-j\pi/2}(T/\tau^2V_{rms}^2)e^{j\omega\tau[1-2\ln(\omega/\omega_0)/(\pi Q_{eff})]}e^{-\omega t/(2Q_{eff})} \ , \tag{6}$$

where $\tau = \{[(x-x_g)^2 + (y-y_g)^2]/V_{rms}^2 + T^2\}^{1/2}$ denotes the traveltime from the receiver to the image point.

From eq. (5), just as V_{rms} expresses the root-mean-square of the interval velocity, Q_{eff} expresses the "mean" absorption from surface seismic data to the imaging point. It is more practical to obtain the wavefield at time depth T with Q_{eff} by eq. (5) than to perform a spatial Fourier transform of eq. (3) with interval Q, which is a recursive solution above all the layers above the time layer T and hence results in a huge computational cost. Furthermore, Q_{eff} varies smoothly, its first-order derivative is continuous, and it is available to scan Q_{eff}.

Eq. (6) has two Q_{eff}-related terms; $e^{j\omega t[1-\ln(\omega/\omega_0)/(\pi Q_{eff})]}$ denotes the dispersion, meaning that high frequency waves propagate faster than low frequency waves, which alters the shape of wavelet; $e^{-\omega\tau/(2Q_{eff})}$ denotes the amplitude compensation, and as time and frequency increase, the wave compensation increases. The interval Q field can be estimated from the Q_{eff}, obtained by scanning, by applying the inverted eq. (5). With the time-to-depth conversion, we can convert the time interval Q field to a depth interval Q field.

Q ESTIMATION

The effective parameter (Q_{eff}) estimation, which is obtained by Q_{eff} scanning, is necessary to build the interval Q field. The Q_{eff} scanning is carried out by multiple inverse constant Q filtering plus prestack time migration and a subsequent determination. We evaluate the Q_{eff} value of the compensation stack section of inverse Q filtering plus migration. However, real data have ambient noise, which will be boosted in inverse Q filtering, especially for high-frequency noise. Furthermore, noise levels in different locations are different for various reasons, such as seismic layout and data acquisition. Therefore, it is necessary to consider the different noise levels when evaluating the Q value. The suitable Q_{eff} is chosen when its stacked section has better resolution, wider bandwidth, and an acceptable noise level.

Q_{eff} scanning

To scan Q_{eff} more accurately, we take a series of Q, whose reciprocals are equally spaced from the largest to the least. Inverse Q filtering for prestack seismic traces can compensate for absorption and dispersion, and then the prestack time migration will supply stacked sections to evaluate the Q_{eff} value. Using phase shift (Gazdag, 1978), the inverse Q filtering of the first-order time derivative of the seismic trace may be presented as:

$$p(t) = \int F(\omega)\omega e^{-j\pi/2} e^{j\omega t[1-\ln(\omega/\omega_0)/(\pi Q_{eff})]} e^{\omega t/(2Q_{eff})} d\omega \quad , \tag{7}$$

where the phase shift operator is:

$$\phi(\omega,t) = e^{j\omega t[1-\ln(\omega/\omega_0)/(\pi Q_{eff})]} e^{\omega t/(2Q_{eff})} \quad .$$

Then, the conventional Kirchhoff migration formula of an input trace is:

$$I(x,y,T) = (\tau_s/\tau_g)^2 p(\tau_s + \tau_g) \quad , \tag{8}$$

where τ_s and τ_g are the travel times in a lossless medium from the image point (x,y,T) to the source and receiver, respectively. Substituting eq. (7) into eq. (8), we have a migration impulse response of a seismic trace; that is:

$$I(x,y,T) = (\tau_s/\tau_g)^2 \int F(\omega)\omega e^{-j(\pi/2)} e^{j\omega(\tau_s+\tau_g)[1-(1/\pi Q_{eff})\ln(\omega/\omega_0)]} \times e^{\omega(\tau_s+\tau_g)/2Q_{eff}} d\omega \quad . \tag{9}$$

When Q_{eff} are all constants across the whole field, it can be proven that eq. (8)

is de-absorption prestack time migration (PSTM). In eq. (8), if Q_{eff} tends to infinity, the compensation term in the frequency integral tends to be 1, and the dispersion tends to be $e^{j\omega(\tau_s+\tau_g)}$. Therefore, eq. (8) is reduced to the conventional PSTM.

In contrast with eq. (9), eqs. (7) and (8), the prestack inverse Q filtering plus PSTM, significantly reduce the computational cost because the summation over frequencies at each image point in eq. (9) is replaced with the summation over frequencies at each temporally sampled point. In addition, in the numerical computation of eq. (7), the phase shift operator of a different time at a given frequency can be computed with an iterative algorithm to reduce computational cost; that is:

$$\phi(\omega,t_{i+1}) = \phi(\omega,t_i)k \quad ,$$

$$k = e^{-j\Delta\omega t[1-\ln(\omega/\omega_0)/(\pi Q_{eff})]}\, e^{\omega t/(2Q_{eff})} \quad ,$$

where k is a constant if ω is invariant at every iteration. Therefore, inverse Q filtering plus PSTM makes it practical and stable to scan Q effectively.

Spectral bandwidth and tuning effects

The spectrum is an important index (mainly the spectral bandwidth) in Q_{eff} estimation, with which two continuous wavelets reflected from a single thin layer would interfere. These interferences strongly alter the spectrum and result in spectral notches. Fig. 1 shows the altered spectrum of two Ricker wavelets reflected from the top and bottom interfaces of a single thin bed, respectively. It is troublesome to measure the bandwidth of the distorted spectrum, and the dominant frequency moves forward. The contaminated spectra will also seriously influence the effectiveness of the conventional methods of Q estimation; the notches will cause instability in the spectrum-ratio methods, and the dominant frequency moving forward will cause some anomalies on the frequency-shift related methods.

To eliminate the interference effects on the measurement of the spectral bandwidth, we proceed as follows. When selecting the spatially sampled point, we choose a time-space window of multiple CDPs instead of a time window at one CDP. The spectrum of the time-space window is a stacked spectrum of the entire traces in the window, and it is relatively smooth with few notches. When choosing the window, we prefer the place where its frequency component is abundant and try to avoid the places where its event is strong and is mainly about harmonics, which may lead to a single peak frequency in its spectrum. The time duration is about five cycles of the wavelet, and it is an empirical parameter for a real spectrum. The lateral width, which determines the stacked

times of the spectra, is determined by the performance of the spectrum, and the window broadens as the number of notches increases.

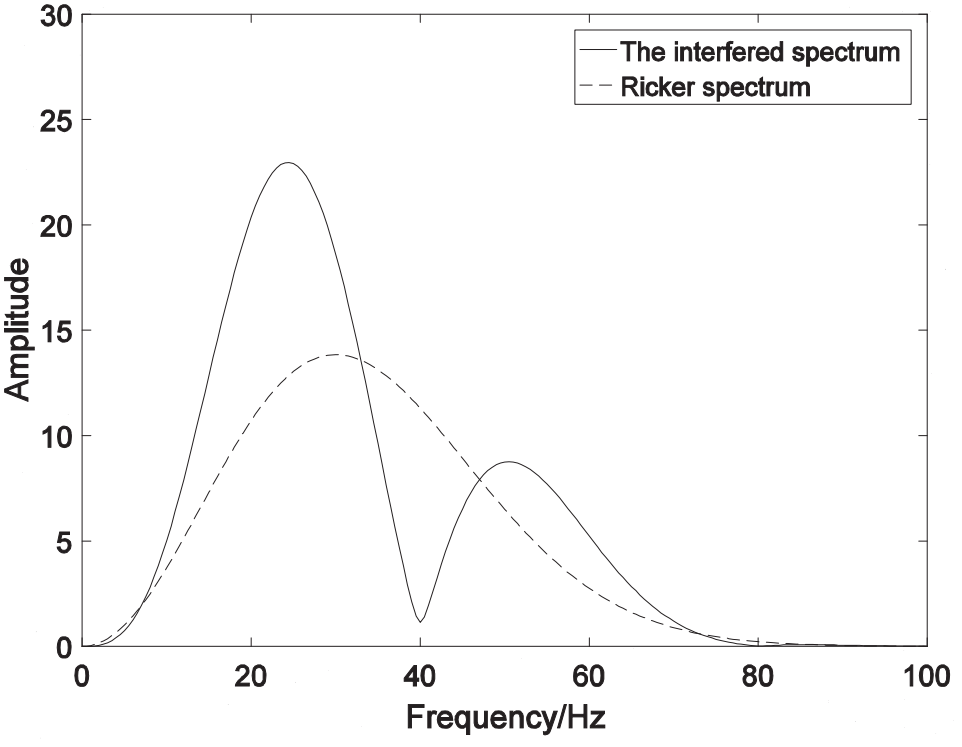

Fig. 1. Illustration of the effects of a single thin layer in the spectra of the Ricker wavelet (solid line) and the interfered wavelet (dashed line).The interfered spectrum is distorted with a notch at 40Hz and its dominant frequency moves forward, which will yield erroneous Q estimation when using the methods depending on spectra or frequency-dependent amplitudes.

As depicted in Fig. 2, this section has several thin layers resulting in terrible interferences. The thickness of the layers is less than the one quarter wavelength, therefore the wavelets reflected by the upper and the lower boundaries overlap and cannot be separated as shown in Fig. 2b, which cause several notches in its spectrum in Fig. 2c (dashed line). The solid line, which denotes the stacked spectrum of the window, has fewer notches and extreme frequencies than that of a single spectrum of the middle CDP, which is denoted by the dashed line. Therefore, it is easier to measure the bandwidth using the stacked spectrum in Fig. 2c.

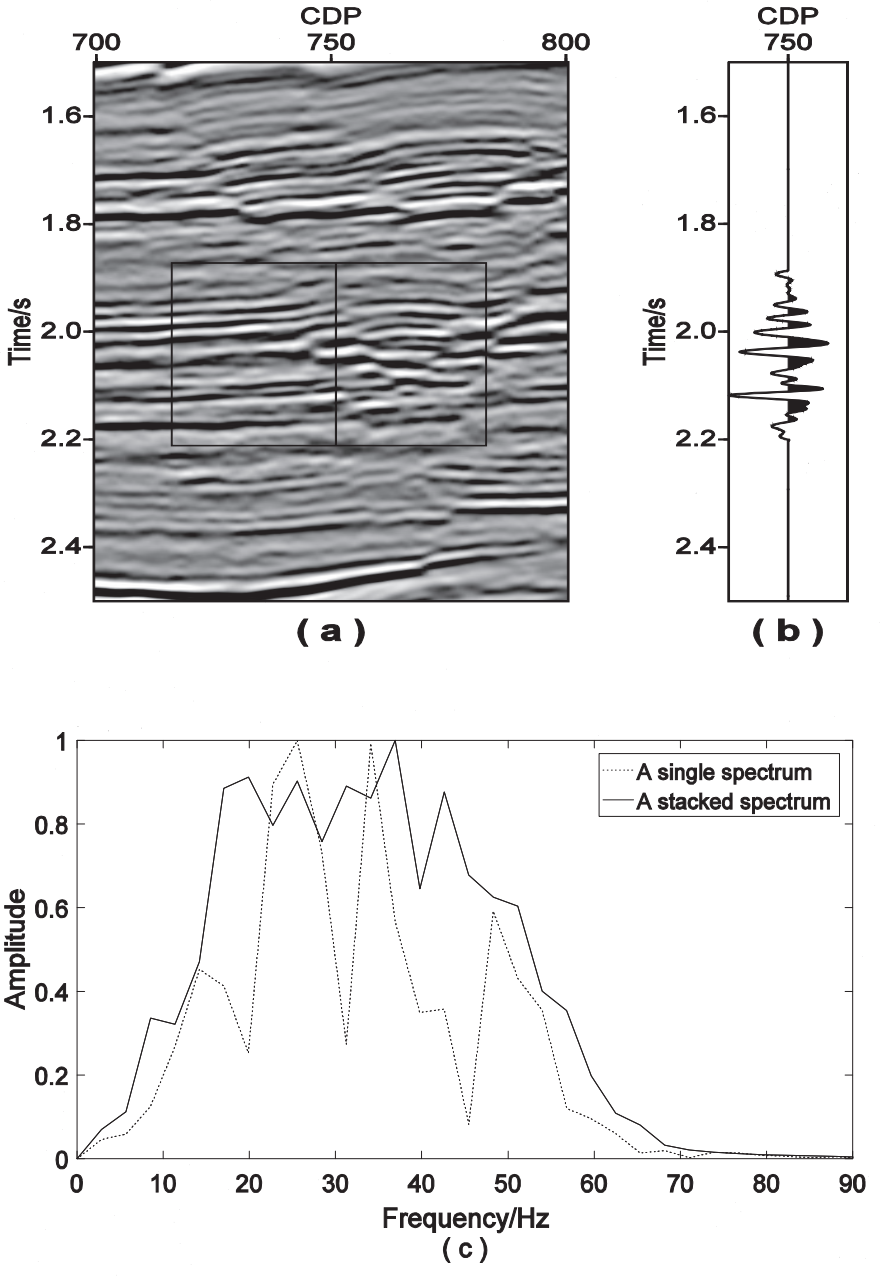

Fig. 2. Illustration of the stacked spectrum and the tuning effect. (a) The selected window for the stacked spectrum in the box. (b) The single trace in middle of the box. (c) Comparison of the spectra between that of a single trace and the stacked spectrum in the box. This section in the window has several thin layers, whose thickness is less than one quarter wavelength, therefore the wavelets reflected by the upper and the lower boundaries overlap and cannot be separated as shown in Fig. 2b, which cause several notches in its spectrum in Fig. 2c (dashed line). The solid line, which denotes the stacked spectrum of the window, has fewer notches and extreme frequencies than that of a single spectrum of the middle CDP, which is denoted by the dashed line in Fig. 2c.

High-frequency noise control

Q compensation enhances the high frequency components and suppresses the low-frequency components, which would boost high-frequency noise because the signal of the high frequency component has been attenuated to a level below the noise level. Fig. 3 shows the compensated spectrums of an attenuated wavelet in which Q equals 100. When the Q used in compensation is 100, the high frequency noise is ambient and the performance is poor, which make it troublesome to pick Q. Thus, it is necessary to compare the different Q-compensated sections at the same noise level. To quantify the high-frequency noise level, we try to separate the noise from the compensated sections through filtering. We prefer a filtering algorithm based on a local polynomial approximation (Lu et al., 2006) due to the continuity of events rather than low-pass filtering, which would eliminate the high frequencies we intend to recover. Therefore, we define a parameter related to a specific frequency range,

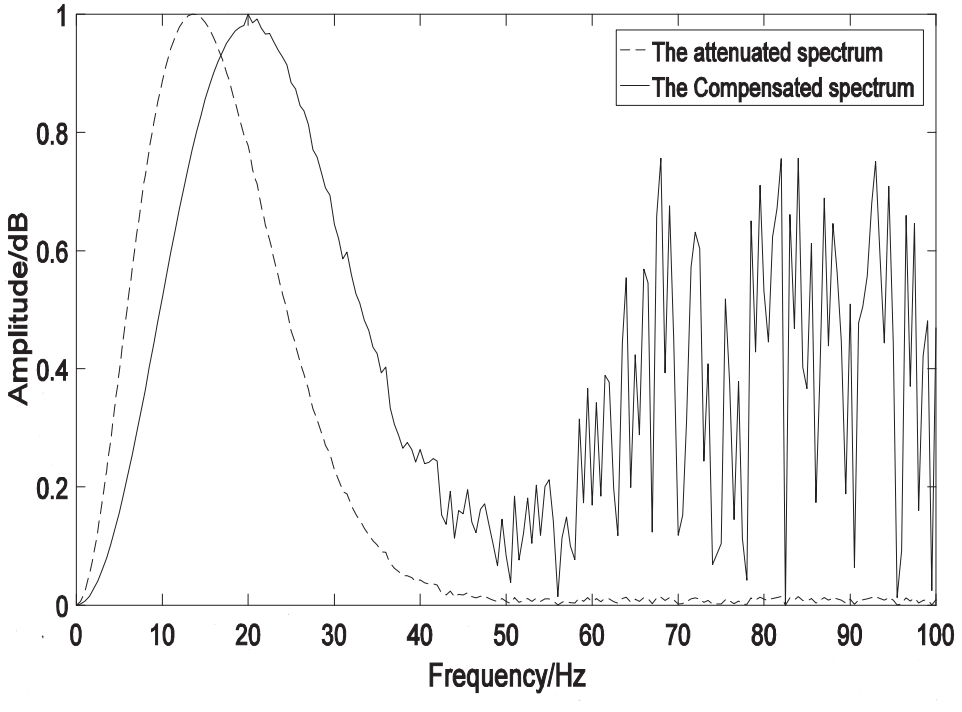

Fig. 3. Comparison of the Wavelets' spectra with high-frequency noise. The dashed line is the spectrum of the initial and attenuated wavelet with high-frequency noise. The solid line is the compensated spectrum with the correct Q (Q = 100). The high-frequency noise, which is not ambient over 50 Hz in the initial wavelet, is boosted after compensation.

$\zeta(f_c)$, to evaluate the noise level of the compensated section within the picked window; that is:

$$\zeta(f_c) = \int_{f_r}^{f_c} A_n^2(f)df \; / \; \int_{f_r}^{f_c} A_s^2(f)df \; . \tag{10}$$

where A_n is the amplitude spectrum of the noise, and A_s is that of the signal, which can be obtained by subtracting noise from signal. f_r is the starting reference frequency and is usually the dominant frequency, and f_c is the cut-off frequency in compensation. Thus, $\zeta(f_c)$ varies with the cut-off frequency and Q value. When keeping $\zeta(f_c)$ invariant, we make all the noise levels of different Q-compensated sections reasonable; the different Q values correspond to different cutoff frequencies, which mainly influence the bandwidth of the spectra.

In addition to measuring the effective bandwidth in the frequency domain, we can also evaluate the Q value in the time domain by focusing on the features

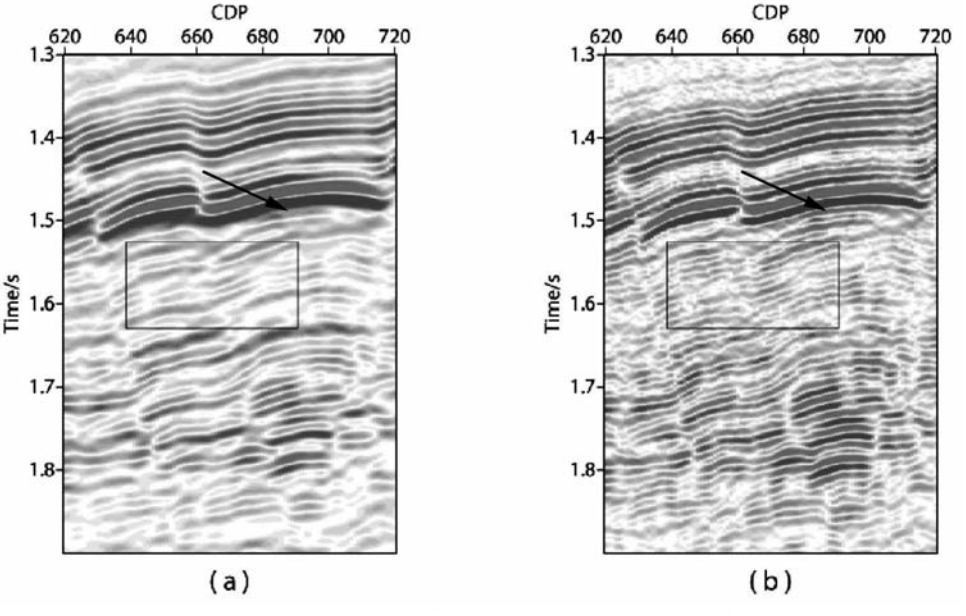

Fig. 4. Comparison between the local sections with different Q compensation. Part (a) uses a larger Q and Part (b) uses an appropriate Q. The compensated section, part (b), indicated in the rectangle has higher resolution, and the overlay events are well separated, while part (a) under compensation has lower resolution. The thin event, which is calibrated by the interpreter, noted by the arrow, is well-imaged in part (b).

of the events. As depicted in Fig. 4, the compensated section (Fig. 4b) with a suitable Q indicated in the rectangle has higher resolution, and the overlay events are well separated, while Fig. 4a under compensation has lower resolution. The thin event, which is calibrated by the interpreter, noted by the arrow is well-imaged in Fig. 4b.

BUILDING THE Q FIELD

Once vertically varying sampled points of Q_{eff} in one CDP are obtained, we can convert Q_{eff} to interval q (the lowercase of q denotes interval Q while the capital of Q denotes the Q_{eff} in this chapter) by inversion, according the following formula:

$$q_i = (T_i - T_{i-1})/[(T_i/Q_i) - (T_{i-1}/Q_{i-1})] \quad . \tag{11}$$

In eq. (11), T_i/Q_i can be less than T_{i-1}/Q_{i-1}, which will result in the unreasonable interval q. To avoid this problem, we compute the interval immediately and constrain the interval q in the reasonable range of 40 ~ 2000, when selecting the effective Q.

It is not practical to scan every CDP, which is a huge workload, and we only sample several CDPs in the direction of the survey line. For these areas not sampled, we obtain the interval q by lateral interpolation, which is associated with geological interfaces. The field of primary velocity, which can be built by velocity scanning before inverse Q filtering, is generally recognized to be positively correlated with the q field, and it can map the geological interfaces grossly. Thus, we put forward an algorithm based on the following empirical formula (Waters, 1978) to interpolate the interval q using the velocity field and proceed in three steps.

First, we derive the positive relationship between the primary velocity (v) and Q from the empirical formula; that is:

$$q(t,x,y) = \alpha v(t,x,y)^{\beta} \quad . \tag{12}$$

Taking the logarithm of both sides yields

$$\ln[q(t,x,y)] = \ln(\alpha) + \beta \ln[v(t,x,y)] \quad , \tag{13}$$

where α and β are empirical parameters in a working area and could be different in different blocks of an oil field, and the velocity is in units of km/s. Eq. (13) validates the linear relationship between and ln(q) and ln(v) then the two parameters can be obtained by linear regression, where $\ln(\alpha)$ denotes the

intercept and β denotes the slope. The scatter diagram (Fig. 5) shows the regression results (α = 11.03; β = 2.2) from the real data of an oil field, which is similar to that of Waters (1978).

Next, although the q field can be achieved by eq. (12), the q values on the sampled CDP deviate from the more reliable scattered points, which are well estimated and evaluated. To correct this deviation between the scattered points and the regression line, we introduce another 3D parameter, m, which is called the correction coefficient and is defined as:

$$m(t,x,y) = q_p(t,x,y)/[\alpha v(t,x,y)^{\beta}] \quad , \tag{14}$$

where q_p is the interval q selected on the sampled CDP and m is a constant, 1, when the scatter point is located on the regression line. The whole 3D correction coefficient field over the entire imaging volume can be achieved by lateral interpolation at each lateral position and a subsequent process of smoothing.

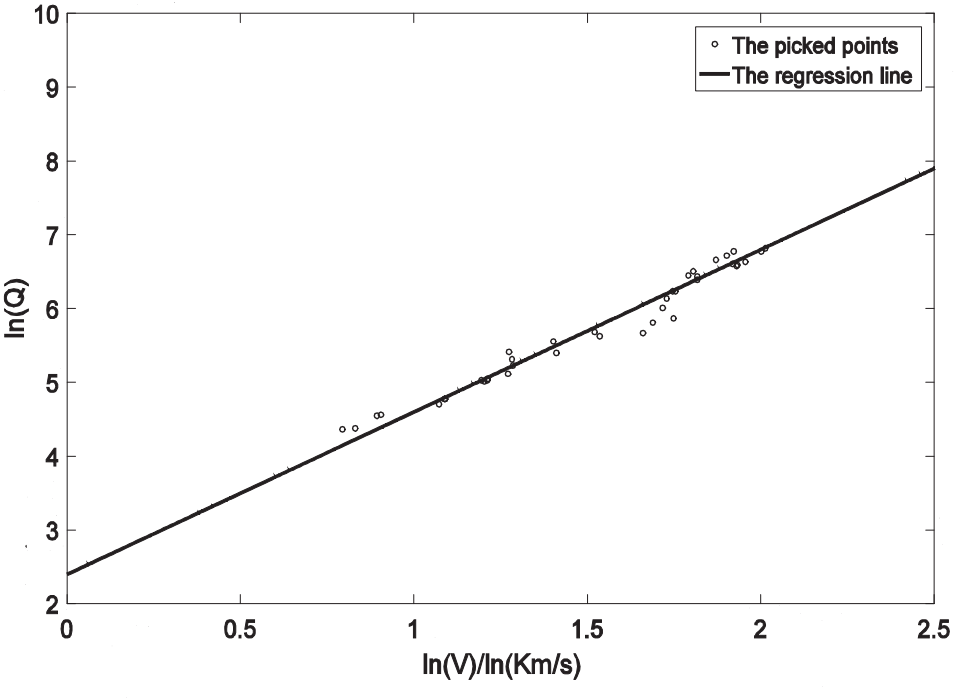

Fig. 5. The two empirical parameters in eq. (12), α and β, can be obtained from linear regression of the scatter points of [ln(v),ln(Q)], where ln(α) denotes the intercept and β denotes the slope.

Last, the q value at each point is the product of the correction coefficient and the computed q using the empirical eq. (12); that is:

$$q(t,x,y) = \alpha v(t,x,y)^{\beta} m(t,x,y) \quad . \tag{15}$$

The interval q field in Fig. 6, obtained by this interpolation algorithm, is consistent with the velocity field, which achieves the expected effect, and the effective Q field can be obtained by the integrating the interval q field. It can be used in the de-absorption prestack time migration directly or in the de-absorption prestack depth migration with the proper time to depth conversion (Maria Cameron, 2008). Therefore, the interval q field in depth in Fig. 7a, converted from that in Fig. 6, is related with the interval velocity in depth in Fig. 7b and can be used for the de-absorption prestack depth migration.

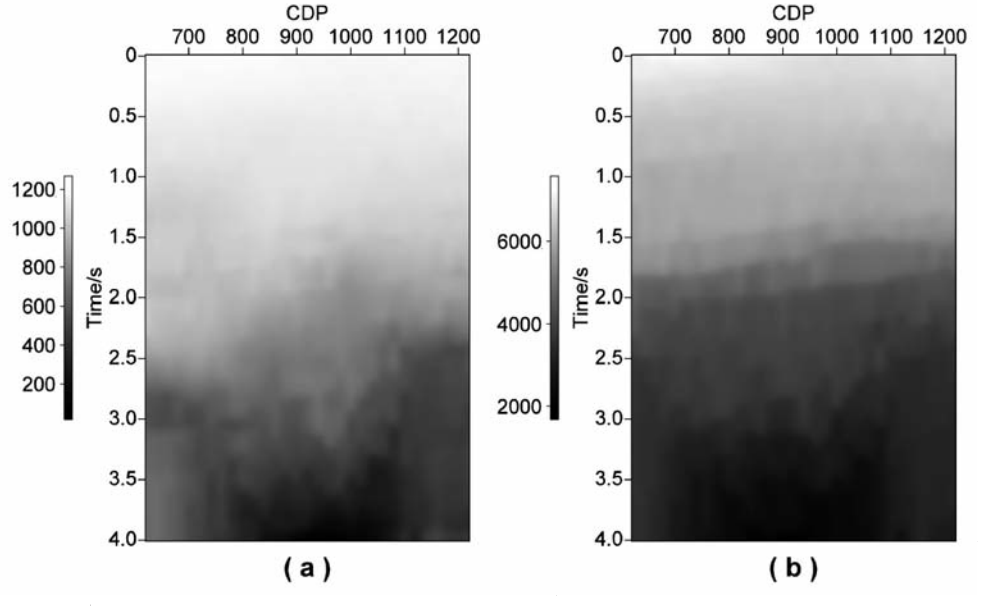

Fig. 6. The interval Q field (a), obtained using the geology-constrained algorithm of interpolation, is consistent with the interval velocity field (b) in the time domain. It has similar changes with the velocity field, which maps the structural shape of the subsurface grossly.

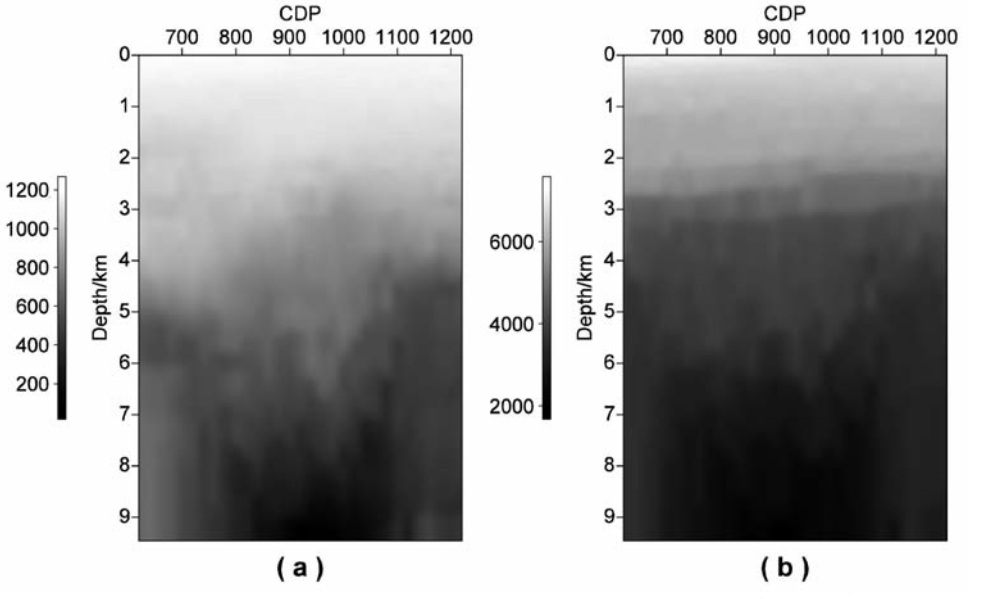

Fig. 7. The interval Q (a) in depth, converted from that in Fig. 6a, is related with the interval velocity in depth in (b) and can be used for the de-absorption prestack depth migration.

WORKFLOW AND A REAL DATA EXAMPLE

The workflow to build a heterogeneous Q model is summarized briefly as follows:

1. Select sampled points. Several important CDPs are chosen, followed by a determination of the time windows on the events of the target strata from shallow to deep on the conventional migration stacked section.

2. Perform the inverse Q filtering plus prestack time migration.

3. Determine the acceptable high-frequency noise level and evaluate the Q_{eff} on the frequency and time domain.

4. Convert Q_{eff} to interval Q and obtain empirical parameters and by linear regression.

5. Compute the correction coefficients. The whole field is achieved by lateral interpolation on these sampled CDPs at each depth point and a subsequent smoothing process.

6. Yield the Q field based on eq. (12).

We further apply our methodology to a real dataset of an oil field in eastern China, which is characterized by almost horizontal strata, no geological complex conditions and sandstone reservoirs. With the exploitation of the oil field, the major prospecting target tends to the thin interbeds with serious tuning effects. The primary task for seismic data processing is to improve the resolution of imaging with a heterogeneous field so that horizontal wells are drilled more accurately.

One block of this oilfield is taken as an example, where the shot line spacing is 240 m, the shot spacing is 40 m, the receive line spacing is 160 m, the receiver spacing is 40 m, the bin size is 20 m * 20 m with 114 folds (6 times in the cross-line direction and 19 times in the line direction), and the total data size is 1.3 T. The noise in this working area varies, and a constant Q model is not suitable. Therefore, our method is used to build a heterogeneous Q model for the de-absorption PSTM, and Fig. 8 shows a section of Q_{eff} in one line. Fig. 9a is the local migration section of the conventional PSTM while Fig.9b is that of the de-absorption PSTM. As shown in Fig. 9 and Fig. 10, the resolution of the de-absorption PSTM improves significantly, and its bandwidth increases by approximately 20 Hz.

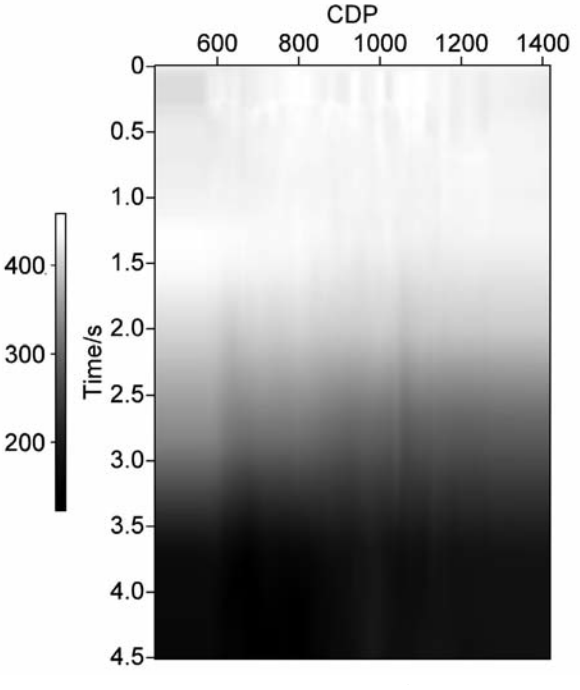

Fig. 8. The section of an effective Q field built from a real data set is heterogeneous and smooth, which is used for de-absorption PSTM.

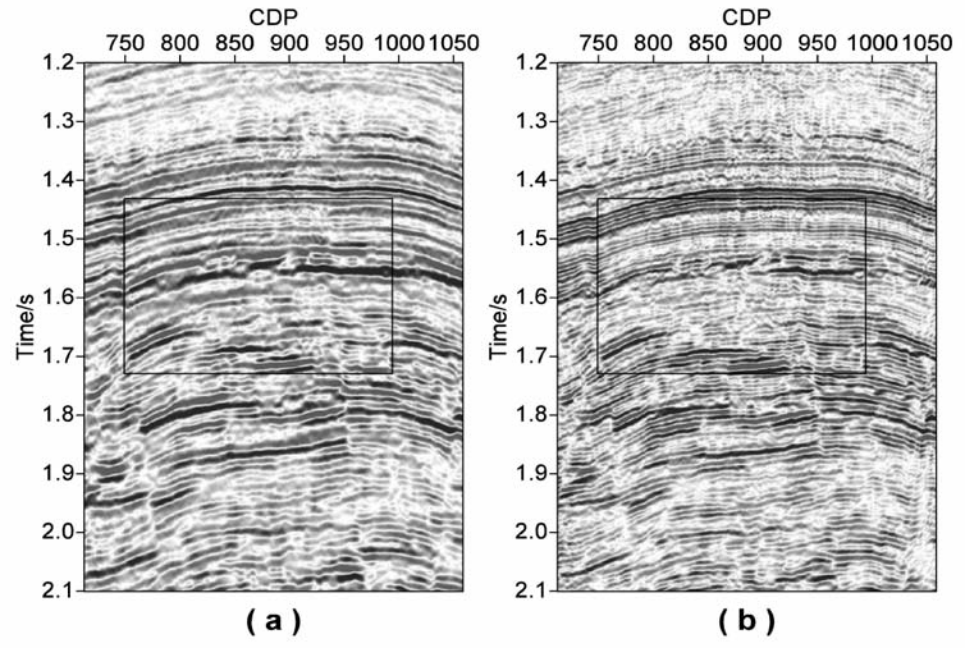

Fig. 9. Comparison between the migration results by (a) the conventional PSTM and (b) the de-absorption PSTM. The resolution of the de-absorption PSTM improves significantly with sharper events.

CONCLUSIONS

We have presented a method to build a heterogeneous Q model using seismic reflection data when VSP data and cross-well data are insufficient. The effective Q, which can be estimated by Q scanning through inverse Q filtering plus convention migration, is introduced to replace the interval Q in deriving wave continuation. Thus, the problem of interval Q estimation is translated to that of effective Q estimation. We evaluate the effective Q value in terms of compensation effects along with imaging resolution and wide bandwidth, while the high-frequency noise level is reasonable. The whole Q model is achieved using a geology-constrained algorithm of interpolation on the selected CDP. This methodology is widespread in an oil field in the east of China, and it has achieved high-resolution depiction of the sandstone reservoirs, which helps to locate the horizontal wells for development and validates the effectiveness of this method.

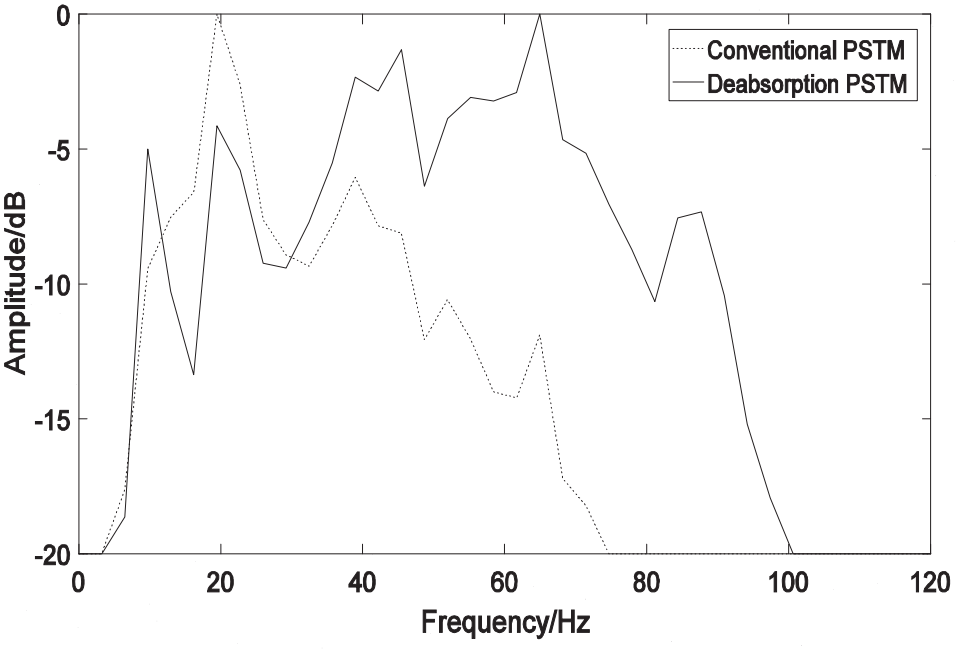

Fig. 10. Comparison between the spectra in the rectangle of Fig. 9 by a conventional PSTM (the dashed line) and a de-absorption PSTM (the solid line).The spectrum of de-absorption PSTM has a wider bandwidth.

ACKNOWLEDGEMENTS

We thank the National Natural Science Fund of China (under grant 41330316) for supporting this work. We thank the editor, and the anonymous reviewers for their important comments and suggestions.

REFERENCES

Aki, K. and Richards, P.G., 1980. Quantitative Seismology. W.H. Freeman & Co, San Francisco.

Bickel, S.H. and Natarajan, R.R., 1985. Plane-wave Q deconvolution. Geophysics, 50: 1426-1437.

Bleistein, N., 1984. Mathematical Methods for Wave Phenomena. Academic Press Inc., New York.

Futterman, I.W., 1962. Dispersive body waves. J. Geophys. Res., 67: 5279-5291.

Hargreaves, N.D. and Calvert, A.J., 1991. Inverse Q filtering by Fourier transform. Geophysics, 56: 519-527.

Kjartansson, E. 1979. Constant Q-wave propagation and attenuation. J. Geophys. Res., 84: 4737-4748.

Lu, W.K., Zhang, W.P. and Liu, D.Q., 2006. Local linear coherent noise attenuation based on local polynomial approximation. Geophysics, 71: V163-V169.

Cameron, M., Fomel, S. and Sethian, J., 2008. Time-to-depth conversion and seismic velocity estimation using time-migration velocity. Geophysics, 73: VE205-VE210.

Mittet, R., Sollie, R. and Hokstak, K., 1995. Prestack depth migration with compensation for absorption and dispersion. Geophysics, 60: 1485-1494.

Youli, Q. and Harris, J.M., 1997. Seismic attenuation tomography using the frequency shift method. Geophysics, 62: 895-905.

Dasgupta, R. and Clark,R.A., 1998. Estimation of Q from surface seismic reflection data. Geophysics, 63: 2120-2128.

Rainer, T., 1989. Comparison of seven methods for the computation of Q. Phys. Earth Planet. Inter., 55: 259-268.

Wang, Y., 2002. A stable and efficient approach of inverse Q filtering. Geophysics, 67: 657-663.

Wang, S., Yang, D., Li, D.F. and Song, H.J., 2015. Q factor estimation based on the method of logarithmic spectral area difference. Geophysics, 80: V157-V171.

Waters, K.H., 1978. Reflection Seismology: A tool for Energy Resource Exploration. John Wiley and Sons, New York.

Zhang, C.J. and Ulrych, T.J., 2002. Estimation of quality factors from CMP records. Geophysics, 67: 1542-1547.

Zhang, J.F. and Wapenaar, C.P.A.. 2002. Wavefield extrapolation and prestack depth migration in anelastic inhomogeneous media. Geophys. Prosp., 50: 629-643.

Zhang, J.F., Wu, J.Z. and Li, X.Y., 2013. Compensation for absorption and dispersion in prestack migration. An effective Q approach. Geophysics, 78: S1-S14.